International Journal of Nuclear Security

Volume 9
Number 2 *ICEP 2022 Conference Papers*

Article 8

7-2024

Thermal Hydraulic Analysis for Different Subchannels of Generic VVER-1200

Mosaddak Ahamed Zahid
Military Institute of Science and Technology, Bangladesh

Md. Imam Mehedi
Military Institute of Science and Technology, Bangladesh

Shamsul Arefin Shibly
Military Institute of Science and Technology, Bangladesh

A. S. Mollah
Military Institute of Science and Technology, Bangladesh

Recommended Citation

Zahid, Mosaddak Ahamed; Mehedi, Md. Imam; Shibly, Shamsul Arefin; and Mollah, A. S. (2024) "Thermal Hydraulic Analysis for Different Subchannels of Generic VVER-1200," *International Journal of Nuclear Security*: Vol. 9: No. 2, Article 8.
https://doi.org/10.7290/ijns09147839
Available at: https://trace.tennessee.edu/ijns/vol9/iss2/8

International Journal of Nuclear Security, Vol. 9, No. 2, 2024—ICEP 2022 Conference Papers

Thermal Hydraulic Analysis for Different Subchannels of Generic VVER-1200

Mosaddak Ahamed Zahid, Md. Imam Mehedi, Shamsul Arefin Shibly, and A. S. Mollah
Department of Nuclear Science and Engineering, Military Institute of Science and Technology, Mirpur Cantonment, 1216-Dhaka, Bangladesh

Abstract
The demand for nuclear energy is steadily increasing all over the world. Most nuclear power is used for peaceful applications such as power generation, healthcare, agriculture, food security, industry, and research. One of the primary applications of nuclear energy is the generation of electricity through nuclear power plants based on nuclear reactors. Many developing countries around the world (such as Bangladesh) are moving toward nuclear power plants because they have huge advantages, including low-cost energy, reliable energy sources, zero carbon emissions, and high energy concentration. As a result, the demand for nuclear reactor protection and operational protection of nuclear power plants is growing rapidly around the world. To meet this demand, nuclear reactor safety as well as nuclear reactor safety parameters must be analyzed. Our research included an examination of the turbulent flow of coolant water into different subchannels of the VVER-1200 nuclear reactor at a pressure of approximately 16 MPa. The Rooppur Nuclear Power Plant, which is currently being built at Ishwardi, an upazila (i.e., subdistrict) of the Pabna District on the bank of the river Padma in Bangladesh, has a VVER-1200 reactor with geometry details of fuel rods, a coolant subchannel, and other operating parameters that are similar to those of that reactor. We used the ANSYS turbulence model to analyze the three subchannels—central, corner, and edge—using three fuel rods. The effects of turbulent flow on temperature distribution, velocity variance, pressure drop, friction factor, Reynolds number, and more were examined in different subchannels of the VVER-1200. The thermal-hydraulic characteristics of coolant water were also investigated to evaluated safety concerns, such as hot spots in the coolant channel and departure from nucleate boiling.

DOI:

Keywords: Reynolds number, subchannel, turbulent flow, friction factor, k–ω, departure from nucleate boiling, shear stress transport, k–ϵ

1. Introduction

The thermal-hydraulic behavior of the fuel assemblies is a critical aspect of a reactor's coolant system. In this study, we conducted a thermal-hydraulic analysis focusing on the behavior of different subchannels of a generic VVER-1200 pressurized water reactor. The results of this analysis will be used to better comprehend how subchannels behave thermally and hydraulically, which will contribute to the overall safety and smooth operation of nuclear power plants. The VVER-1200 is a type of pressurized water reactor that is currently being used in several countries, including Russia and China [1]. The reactor is characterized by its large power output and advanced safety features. However, the thermal-hydraulic characteristics of the subchannels in this type of reactor are not well-understood, and further research is needed to ensure both safe and effective operation. One of the most crucial elements of this research involves establishing safe operation of Bangladesh's biggest project—the Rooppur Nuclear Power Plant, which is a VVER-1200–type reactor. The nuclear power plant will have two units, called Rooppur Units 1 and 2, each of which can produce 1200 MW of electricity [2]. The project is being developed with the aim of providing a sustainable and reliable source of electricity to meet the country's growing demand. This research has particular importance to Bangladesh because it can provide valuable insights into the performance of the nuclear power plant, which is critical for ensuring the plant's safe and efficient operation.

Tóth and Aszódi performed an analysis of the heat and flow transfer processes of VVER-440 reactors in a single subchannel and in a rod bundle section by using ANSYS CFX 11.0. In their experiment, the researchers first developed subchannel models and an overall mesh. They performed mesh by using k–ϵ, shear stress transport, SSG Reynolds stress, and BSL Reynolds turbulence models to predict stress and secondary flows. They cross-checked their results against publicly available measurement data from Trupp and Azad, who demonstrated that secondary flows were calculated without a spacer grid to be symmetric to the subchannel borders and with a spacer grid to cross the borders. They chose the BSL Reynolds stress model for further investigation and will work to enhance the full-length bundle model. They performed a 2D simulation, but a 3D study is theoretically conceivable to determine the causes of the discrepancy between the output temperature of the fuel assembly and the temperature obtained with in-core thermocouples [3].

Zihao et al. simulated and analyzed the turbulence flow in a full-scale fuel assembly by using meshes and Simcentre STAR-CCM+ software. They tried to explain the differences in axial velocity between different subchannels and corroborated their data by comparing them with the test data of integer hydraulics of the fuel assembly [4]. Thin et al. examined flow parameters of the VVER-1000 reactor's fuel assembly subchannel using ANSYS software and the computational fluid dynamics approach. Subchannels were divided into several types of meshes and investigated. Appropriate

DOI:

meshes were used to study a fluid turbulence model. The first half of the inquiry looked into the effect of the fuel rod, and the second looked into the effect of the spacer grid [5].

Chih-Hung et al.'s research included "CFD investigating the flow characteristics in a triangular-pitch rod bundle using [the] Reynolds stress turbulence model." To simulate the flow characteristics within the rod bundles and to subsequently investigate the effects of various mesh distributions and pressure strain models on the turbulent mixing, a 3D CFD model with the Reynolds stresses turbulence model was proposed in their paper. This method made it possible for the rod bundle to reasonably collect the secondary flow. Using the ANSYS Fluent solver, they created a 3D CFD model to investigate flow characteristics in the rod bundle using a variety of pressure strain models in response surface model (RSM), including the linear pressure–strain model and the quadratic pressure strain model. They showed that when using both standard and fine meshes, the velocity profiles under consideration were less than 0.3. Also, when using the RSM turbulence model, the secondary flow characteristics within the rod bundle could be reasonably accounted for by the existing CFD model [6].

Shafiqul and Hossain analyzed the thermal-hydraulic behavior between a fuel rod and coolant assuming an annular subchannel was used to plot the temperature distribution considering two scenarios: one with variation in volumetric heat generation and one without variation. However, the simulation results and temperature profiles of the fuel rod, cladding, and outer surface of the fuel rod were not exactly the same as theoretical and experimental values. These different values were shown in their graphs of the temperatures at the fuel centerline, fuel surface, and cladding inner surface [7].

Ahmed et al. compared the heat transfer capability of three different types of nanofluids (Al_2O_3, TiO_2, and GO) in a triangular fuel subchannel. The authors determined the optimal volume fraction for each of the three nanofluids to maximize heat transfer. The work was done by assuming turbulent flow conditions. Additionally, they discussed the effect of particle size, noting that smaller particle sizes enhanced heat transfer. The results showed that a 4% volume fraction of Al_2O_3 in water increased the thermal flow the most and thus raised the thermal safety margin [8].

Thus, the importance of thermal-hydraulic study of subchannels cannot be overstated. In our investigation, we used both the k–ω SST turbulence model and the k–ε turbulence model. The near-wall treatment is where the typical k–ω model performs best. The two conveyed variables are the particular turbulent dissipation rate (ω), which indicates the rate of dissipation per unit of turbulent kinetic energy, and turbulent kinetic energy (k), which indicates the energy in turbulence. The scale of turbulence is also referred to as ω. The SST formation transitions to a k–ε behavior in the free-stream. To determine the degree of turbulence in the flow field, the model k–ε computes four variables: production of turbulent kinetic energy (P_k), turbulent eddy viscosity (μ_t), turbulent kinetic energy (k), and turbulence dissipation rate (ε) [9].

DOI:

This study's goal was to conduct a thorough thermal-hydraulic analysis of the various subchannels of a standard VVER-1200 reactor. The following are the study's precise goals:

1. To develop a model for a generic VVER-1200 reactor using ANSYS
2. To perform an analysis on the variations of temperature, pressure drop, flow rate, and friction factor among the flow channels for different subchannels
3. To provide valuable insights into the potential benefits and limitations of using water in the subchannels of a VVER-1200 reactor and pave the way for further research in this field

2. Equations and Mathematical Expressions

The thermal-hydraulic study of several subchannels of the generic VVER-1200 was conducted using the mathematical expressions and equations shown in this section.

a. Governing Equations

Energy equation

The energy equation in CFD is expressed mathematically as Equation (1):

$$\frac{d(\rho E)}{dt} + \nabla(\rho u E) = \nabla(k \nabla T) + \Phi, \tag{1}$$

where ρ is the fluid density; *E* is total energy per unit volume, which is equal to internal energy plus kinetic energy; *t* is time; *u* is the velocity vector; *k* is the thermal conductivity; *T* is temperature; ∇ is the gradient operator; and Φ is source or sink terms that describe energy transfer owing to chemical reactions and heat transfer by conduction, convection, and radiation [10].

Momentum equation

The equation of momentum in CFD is given by Equation (2):

$$\frac{\partial(\rho u)}{\partial t} + \nabla(\rho \vec{u}) = -\nabla p + \nabla \vec{T} + \vec{f}, \tag{2}$$

where ρ is the density of fluid, $\vec{u}$ is the velocity of fluid, *t* is time, ∇ is the differential operator that calculates the volume flux of a vector field through a surface, *p* is the pressure, $\vec{T}$ is the fluid stress tensor, and $\vec{f}$ is the force of body acting on the fluid, including gravity and other external forces [10].

Single-phase pressure drop equation

The single-phase pressure drop equation is given by Equation (3):

$$\Delta P = \frac{f \times L \times \rho \times v^2}{2D}, \tag{3}$$

DOI:

where Δ*P* is the total pressure drop, *f* is the friction factor, *L* is the subchannel's length, ρ is the fluid density, *v* is the fluid velocity, and *D* is the hydraulic diameter [11].

Reynolds number equation

The Reynolds number (*Re*) equation is given by Equation (4):

$$Re = \frac{\rho \times u \times D_{\mathrm{h}}}{\mu}, \tag{4}$$

where ρ is the density of the fluid, *u* is the velocity, D_{h} is the hydraulic diameter, and μ is the viscosity [12].

Two-phase pressure drop equation

The two-phase pressure drop equation is given by Equation (5):

$$\Delta P = f \times g \times H_{\mathrm{v}}, \tag{5}$$

where Δ*P* is the pressure drop, *f* is the friction factor, *g* is the acceleration owing to gravity, and H_{v} is the void fraction [13].

b. The Standard k–ε Model Equations

A set of mathematical equations called the standard k–ε model equations are used in CFD to simulate turbulence in fluid flow. The k–ε model consists of two transport equations: one for the kinetic energy of the turbulence (*k*) and another for its rate of dissipation (ε) as given by Equations (6) for *k* and (7) for ε:

$$\frac{d(\rho k)}{dt} + \nabla(\rho k U) = P - \varepsilon, \text{and} \tag{6}$$

$$\frac{d(\rho \varepsilon)}{dt} + \nabla(\rho \varepsilon U) = C_{\mu}(P - \varepsilon), \tag{7}$$

where ρ is the fluid density, *t* is time, *U* is the velocity vector, *P* is the turbulence production, ε is the turbulence dissipation rate, C_{μ} is the model constant, and ∇ is the divergence operator [14].

c. The Standard k–ω Model Equations

The Reynolds-averaged Navier–Stokes turbulence model, also known as the standard k–ω turbulence model, uses two equations to depict turbulence in flow. These two equations are the turbulence kinetic energy equation given in Equation (8) and the specific dissipation rate equation given in Equation (9):

$$\frac{dk}{dt} + \nabla(u'k) = P - \varepsilon, \text{and} \tag{8}$$

DOI:

$$\frac{d\omega}{dt} + \nabla(u'\omega) = \sigma k^{2/\omega} - \omega^{2/\tau}, \quad (9)$$

where *k* is turbulence kinetic energy, ω is the specific dissipation rate, *u′* is the turbulence velocity fluctuation, *P* is the turbulence production, ε is the turbulence dissipation rate, σ is the turbulence Prandtl number, *t* is time, and τ is the turbulence time scale [14, 15].

The foundation for the thermal-hydraulic analysis in this work was based on these expressions and equations, which were used to compute the heat transfer rate, pressure drop, heat transfer coefficient, and void percent in various subchannels of the generic VVER-1200.

3. Numerical Model of the Subchannels and Methodology

Each of the 163 fuel assemblies of the VVER-1200 reactor core contained 312 fuel rods. The height of the fuel assembly was 4570 mm, and the height of the power-generating portion of the fuel rod was 3750 mm when the reactor was hot [16, 17]. Only 10% of the length of the fuel rods' power-generating component was contained in the computational domain created for this investigation. The effect of the spacer grid was ignored during calculation. Table 1 includes a list of the precise geometrical parameters.

Table 1. The geometry of the computational domain.

Parameters (from equations)	Value (m)
D_p	0.0091
P	0.01275
L	3.75
D_h (center)	0.006
D_h (edge)	0.01
D_h (corner)	0.004

Figure 1 shows that the subassembly had three subchannels. The three subchannels considered in this paper, detailed in Figure 2, were the center, edge, and corner subchannels.

DOI:

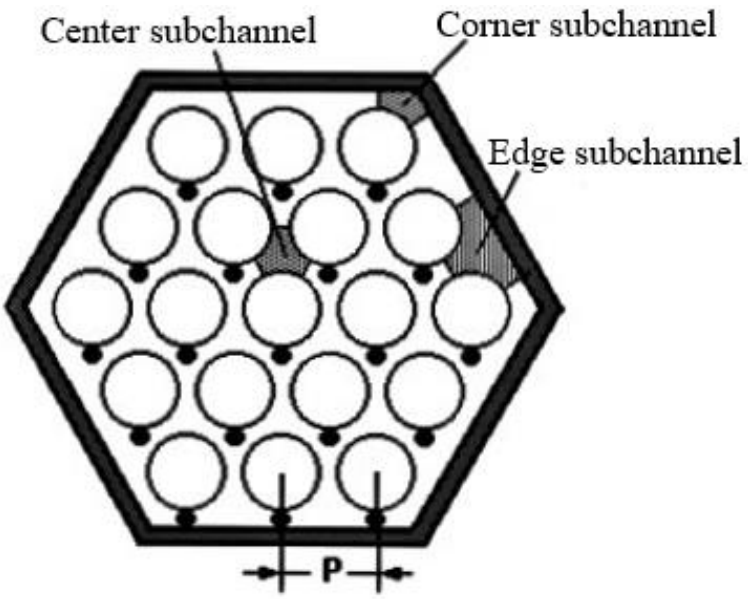

Figure 1. Subchannels of the fuel subassembly.

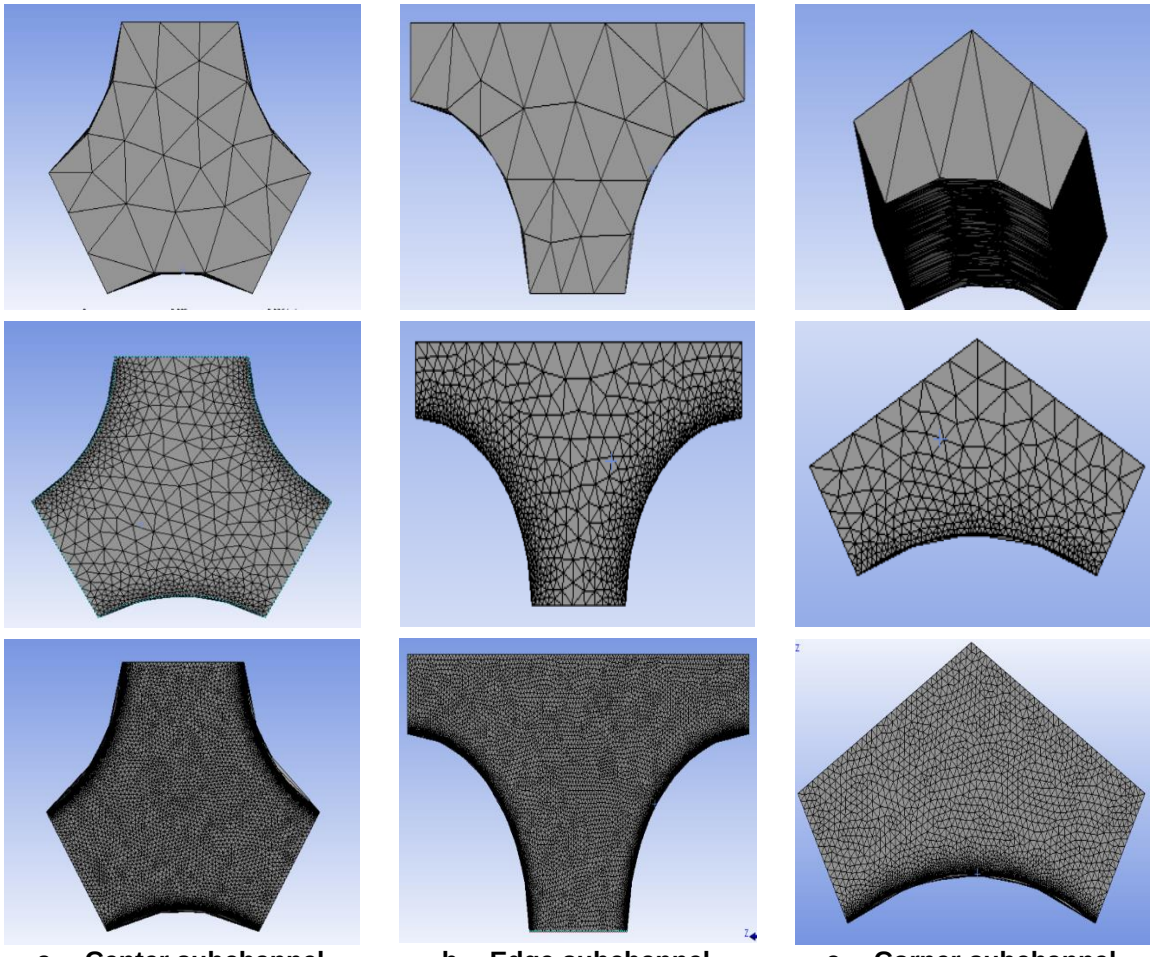

a. Center subchannel **b. Edge subchannel** **c. Corner subchannel**

Figure 2. Outlet subchannels' mesh with different element sizes.

DOI:

Three fuel rods were located in the center subchannel, two were located in the edge subchannel, and one was located in the corner subchannel. The ANSYS FLUENT 2022 R1 program [18] produced the geometry and mesh. The domain elements and nodes for the mesh's three separate subchannels are displayed in Table 2.

Table 2. Characteristics of different subchannel meshes.

	Nodes	Element	Element size (m)	Method
Center	1,552,010	6,266,532	0.001	Tetrahedrons
Edge	1,953,588	7,554,680	0.001	Tetrahedrons
Corner	1,012,219	4,178,388	0.001	Tetrahedrons

4. Results and Discussion

After meshing and setting up the boundary conditions, postprocessing was done in ANSYS Fluent to determine various output parameters necessary for this study. The values of these parameters are described in the following subsections, along with their respective graphical representations.

a. Turbulent Properties

Because of the high Reynolds number, coolant water flow that was moving axially was turbulent. This turbulence significantly influenced the flow characteristics and temperature distribution of the fluid, including kinetic energy, specific dissipation rate, eddy viscosity, and static enthalpy. Figure 3 and Figure 4 indicate that the corner subchannel had a greater concentration of all features than the inner or edge subchannels, as well as a somewhat higher rate of specific dissipation. According to Figure 5, the corner subchannel had a lower concentration of all features than the center or edge subchannels, along with a somewhat lower eddy viscosity. Figure 6 shows that the static enthalpy of the corner subchannel was higher than edge subchannel but lower than the center subchannel. The reason for this difference is the corner subchannel's lower hydraulic diameter, as shown in Table 1, and higher friction factor, which is shown in Figure 11.

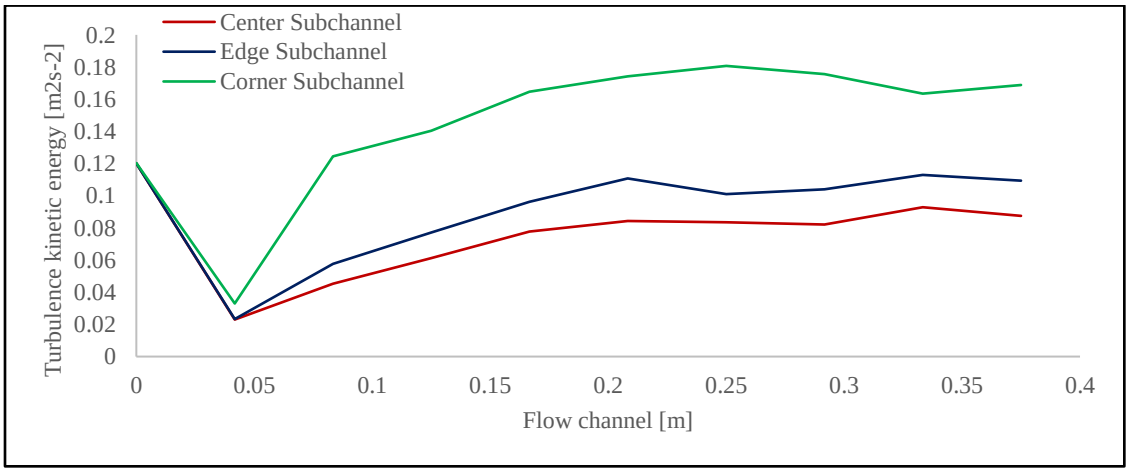

Figure 3. Turbulence kinetic energy along the flow channel in three subchannels.

DOI:

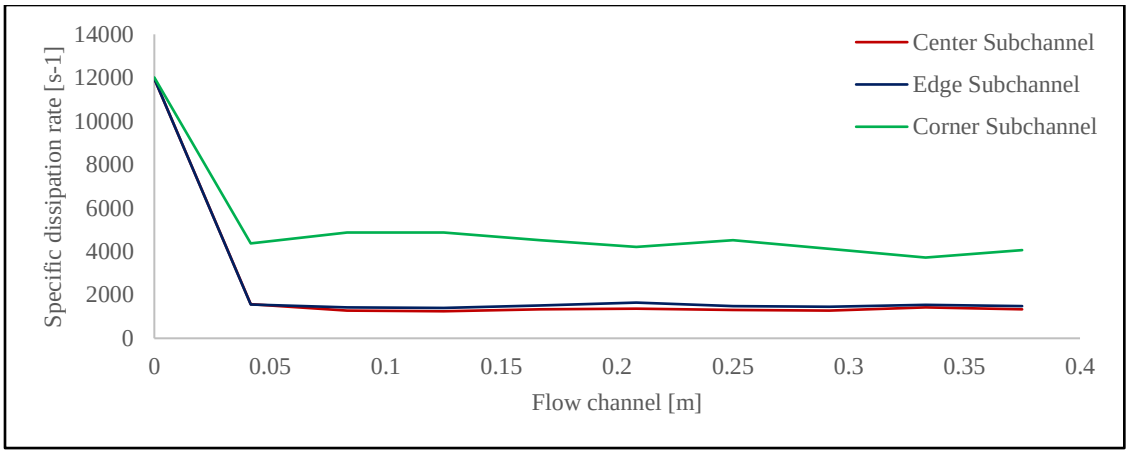

Figure 4. Specific dissipation rate along the flow channel in each of the three subchannels.

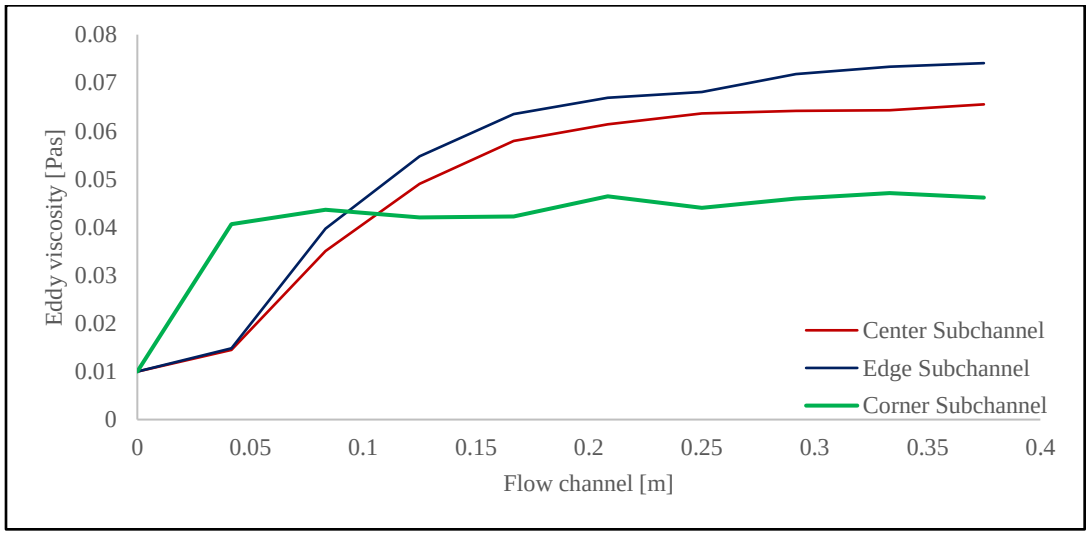

Figure 5: Eddy viscosity along the flow channel in each of the three subchannels.

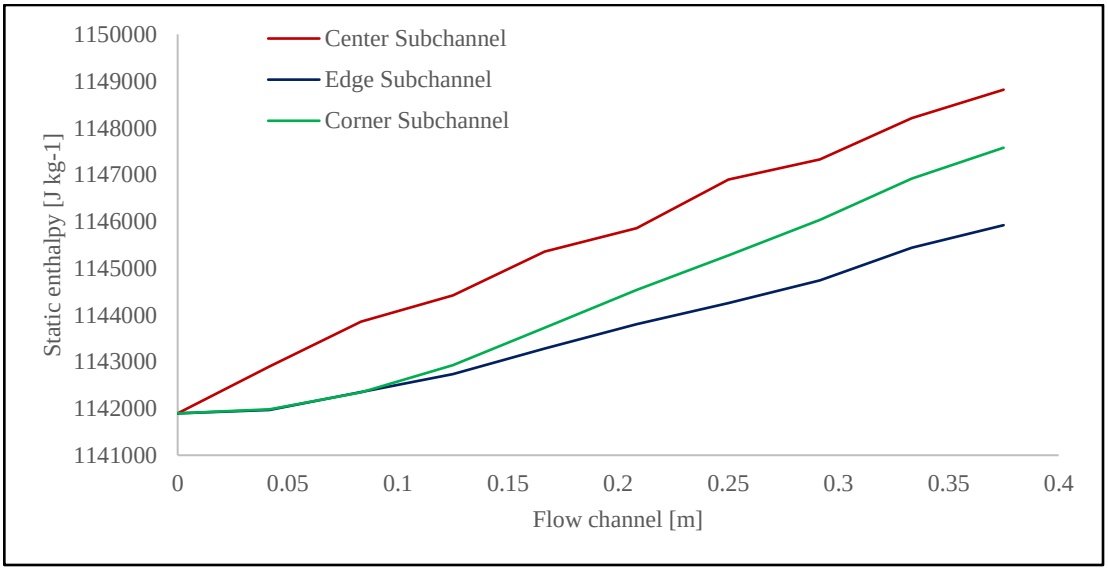

Figure 6: Static enthalpy along the flow channel in each of the three subchannels.

DOI:

International Journal of Nuclear Security, Vol. 9, No. 2, 2024—ICEP 2022 Conference Papers

b. Velocity Distribution

The velocity distribution along the three subchannels is depicted in Figure 7 with a constant inlet velocity of 5.66 m/s. In the first 11.2% of the channel's overall length, the velocities in all the subchannels sharply increased. Then, a progressive increase in velocity occurred along the center and edge subchannels. However, the velocity of the corner subchannel dropped, which can be explained by the corner subchannel's higher turbulence kinetic energy and specific dissipation rates (see Figure 3 and 4, respectively). Additionally, the lower eddy viscosity was another cause of the corner subchannel's drop in velocity, as shown in Figure 5. These drops resulted from the formation of huge eddies and their subsequent splitting into smaller eddies, which caused increasing internal fluid friction in this area more than in other subchannels, thus causing a reduction in the flow velocity of the corner subchannel.

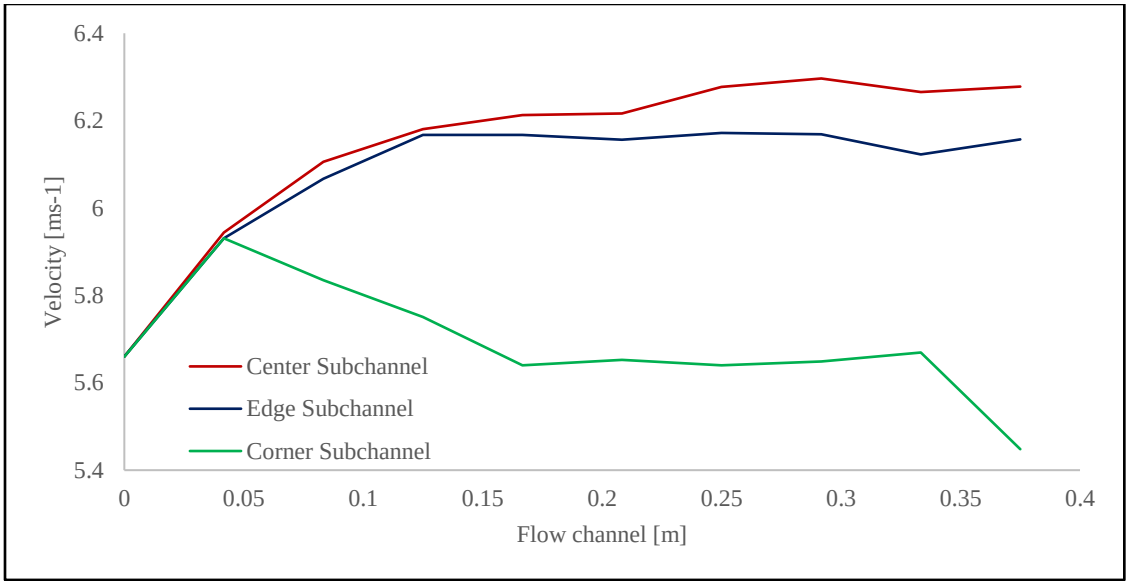

Figure 7. Velocity distribution along the flow channel in each of the three subchannels.

c. Temperature Distribution

Along the flow channel, the distribution of the temperature along the three subchannels is depicted in Figure 8, which shows that coolant temperature remained constant at 571.2 K at the inlet. The temperature rise within the center subchannel was higher than the others because of uniform heat flow. Again, the edge subchannel was surrounded by two fuel rods, and the corner subchannel was surrounded by only one fuel rod. However, specific dissipation rates and static enthalpy were larger angles because of greater temperature rises there. Because the model represents 0.001% of the whole core volume, the average temperature rises of the subchannel in this case was approximately 1.3 K. Extrapolating value to the total reactor capacity, the temperature increase is estimated to range from 20 to 30 K.

DOI:

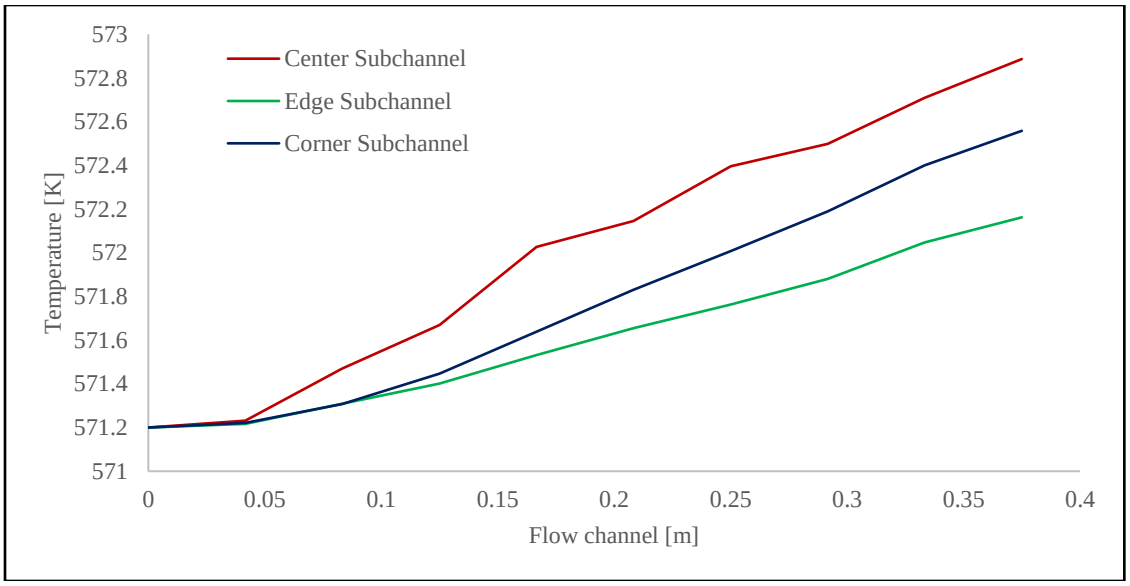

Figure 8. Temperature distribution along the flow channel in each of the three subchannels.

d. Pressure Drop Variation

Standard pressure at the inlet was maintained at 16.2 MPa, and the outflow pressure was constant at 16.19 MPa. The use of water as a coolant resulted in a total pressure drop of 12.9, 13.7, and 54.2 kPa in the center, edge, and corner subchannels, respectively. In all three subchannels, the pressure loss was greater near the inlet and gradually fell along the flow channel. Figure 9 depicts this drop of pressure throughout the flow channel.

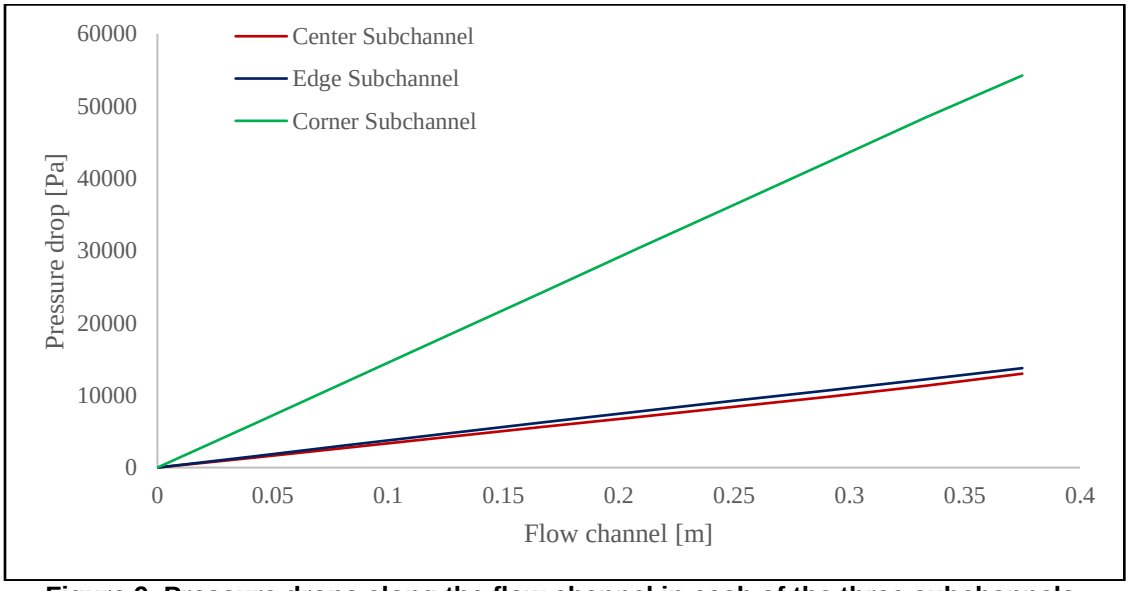

Figure 9. Pressure drops along the flow channel in each of the three subchannels.

e. Reynolds Number and Friction Factor Variation

According to Equation (4), velocity and Reynolds number are related. The hydraulic diameter, D_h, which varied in the three subchannels, determines the Reynolds number.

DOI:

The D_h of the center subchannel was 6 mm, 10 mm for the edge subchannel, and 4 mm for the corner subchannel. The change in Reynolds number is depicted in Figure 10. The greater Reynolds number in the edge subchannel indicates that convective heat transfer occurred here more frequently than in the other two subchannels. In Figure 8, the temperature gradient in the edge subchannel was also found to be less than the other two subchannels. When the D_h is 20 mm, the slope of the edge and center subchannel (Figure10) indicates that the Reynolds number reached its maximum condition. The length of the subchannel must be kept constant for adequate heat removal while considering the minimum length required to achieve a fully developed Reynolds number. In the corner subchannel, the Reynolds number peaked at D_h = 5 and steadily dropped throughout the flow channel. The result indicates a reduction in convective heat transport, but the static fluid enthalpy in the corner subchannel was increasing, as illustrated in Figure 6. The combination of a low Reynolds number and high static fluid enthalpy in at the corner subchannel may result in departure from nucleate boiling (DNB), resulting in two-phase flow, which would reduce the convective heat transfer coefficient.

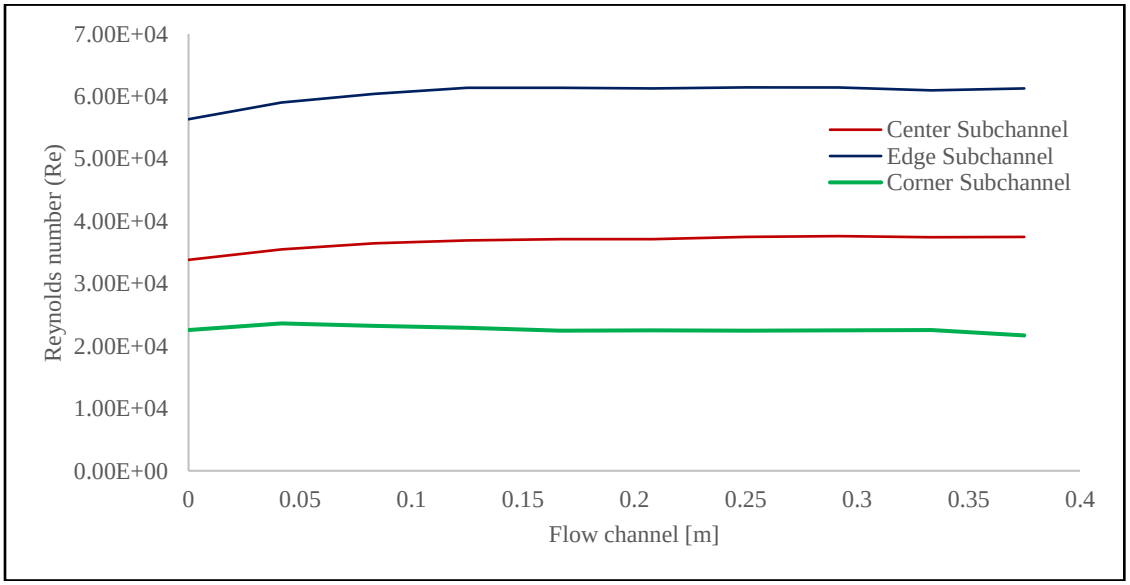

Figure 10. Reynolds number variation along the flow channel in each of three subchannels.

The velocity in various subchannels was used to compute the friction factor. Figure 11 illustrates how the friction factor varied along the three subchannels of the flow channel. Because of a larger coolant flow, the friction factor was higher in the edge subchannel. Interestingly, despite having a smaller area, the additional eddy viscosity in the flow area of the center subchannel caused its friction factor gradient along the flow channel to be higher than that of the corner subchannel.

DOI:

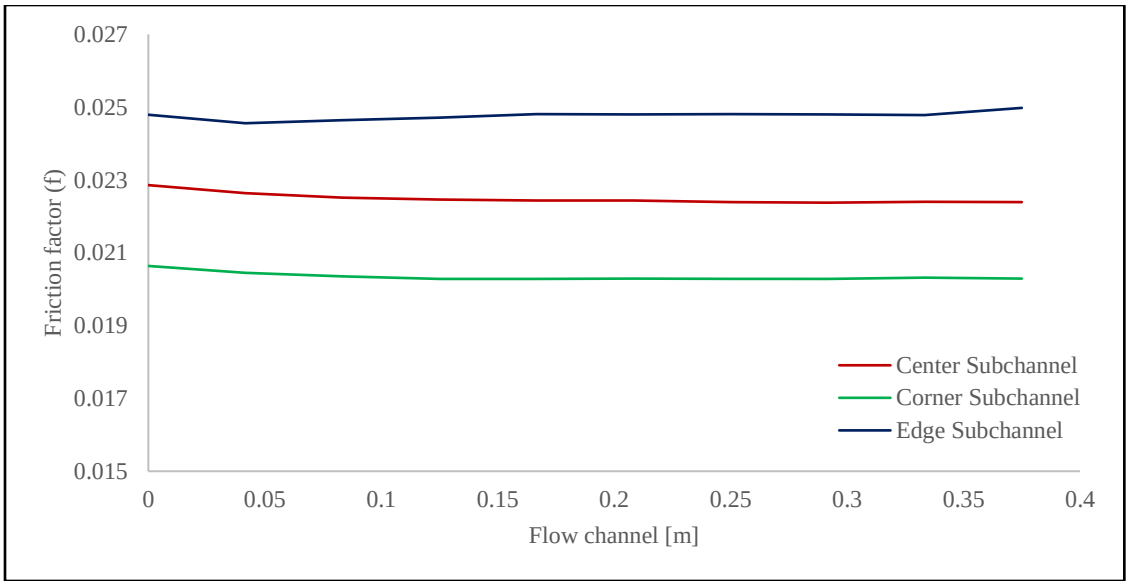

Figure 11. Friction factor variation along the flow channel in each of the three subchannels.

f. Validation

Validation is very important for any simulation model. In this study, validation was done using another model. In this study, the k–ω SST model was used for simulating all working processes, and validation was done by comparing results obtained from the k–ε model. Those results are shown in Figures 12, 13, and 14, which reveal a variation in the velocity, temperature, and pressure drop, respectively, between the k–ω SST and the k–ε models. Although a slight change occurred in the values of velocity, temperature, and pressure drop along the flow channel, the nature of the graph is almost the same between the two models.

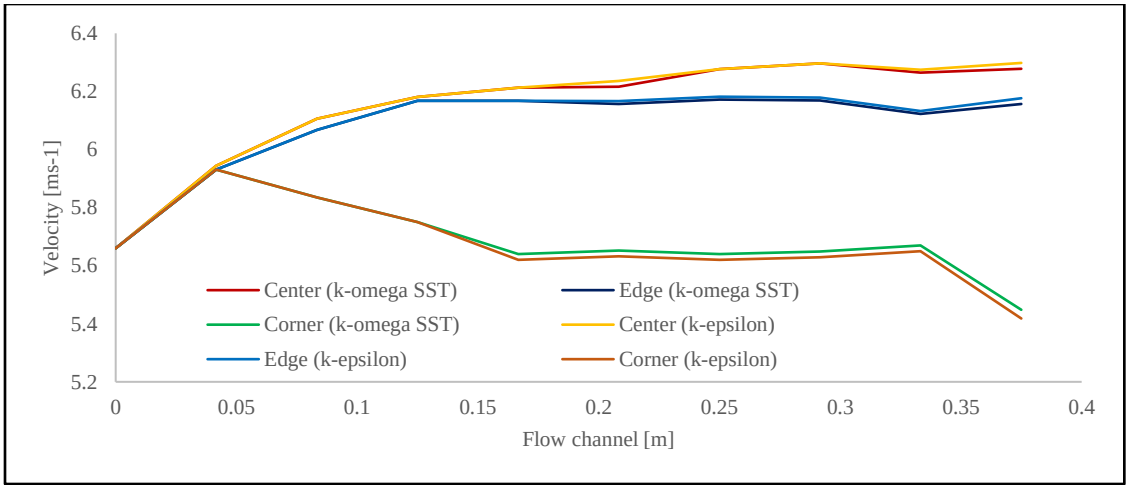

Figure 12. Validation of velocity between k–ω and the k–ε models.

DOI:

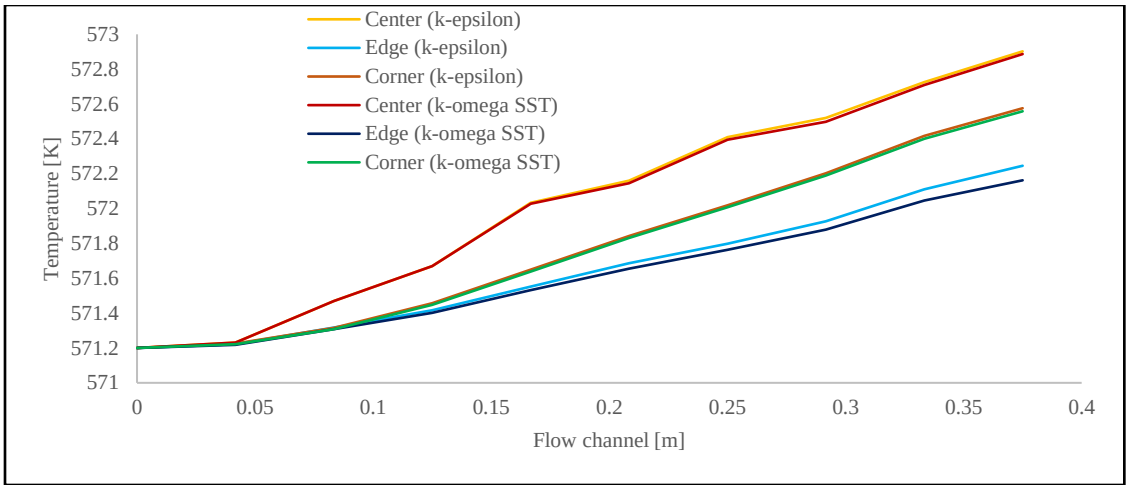

Figure 13. Validation of temperature between k–ω and the k–ε models.

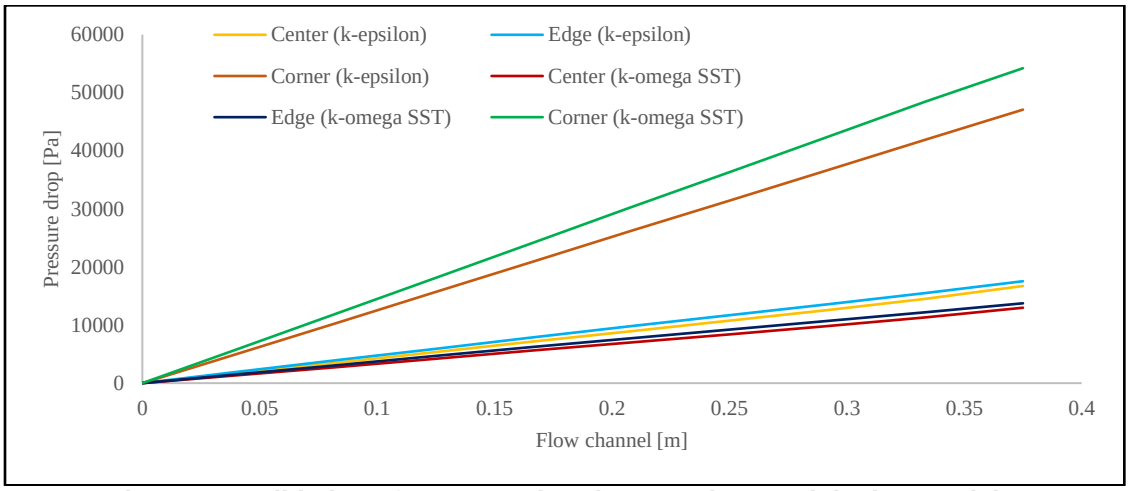

Figure 14. Validation of pressure drop between k–ω and the k–ε models.

5. Conclusion

In this study, we used a nuclear reactor with a 1200 MW capacity to conduct a CFD model test in the center, edge, and corner subchannels of the hexagonal fuel subdivision. The operational parameters of the three subchannels changed sequentially as a result of their various geometrical shapes and edges as well as their effects on the environment of the reactor. From this research, the following conclusions can be drawn:

1. Because of the uniform heat flux the velocity of the center subchannel is greater than the other two subchannels.
2. The turbulence kinetic energy–specific dissipation rate of the corner subchannel is higher because of the roughness of the boundary wall of the core. As a result, velocity fluctuation occurs in the corner subchannel.
3. The relative pressure drop is greater in the corner subchannel. This occurs because of an increased turbulence dissipation rate and a larger volumetric area, resulting in greater temperature distribution in the corner subchannel than the edge subchannel.
4. As a result of a larger coolant flow area, the friction factor is higher in the edge subchannel. Therefore, with a low Reynolds number and high static enthalpy of fluid,

DOI:

DNB may occur at the corner subchannel. A two-phase flow might develop as a result of DNB, which would reduce the convective heat transfer coefficient.

6. References

1. ROSATOM. *The VVER Today: Evolution, Design, Safety*; ROSATOM: Moscow, Russia, 2018. https://www.rosatom.ru/upload/iblock/0be/0be1220af25741375138ecd1afb18743.pdf.
2. Ali, T.; Arnab, I. Z.; Bhuiyan, S. I.; Anik; Rahman; Hossain, I.; Shidujaman, M. Feasibility Study of RNPP(Rooppur Nuclear Power Project) in Bangladesh. *Energy and Power Engineering* **2013**, *5*, 1526–1530. DOI: 10.4236/epe.2013.54B289.
3. Tóth, S.; Aszódi, A. CFD Analysis of Flow Field in a Triangular Rod Bundle. *Nuclear Engineering and Design* **2010**, *240* (2), 352–363. DOI: 10.1016/j.nucengdes.2008.08.020.
4. Yan, Y.; Zhao, T.; He, Z.; Yang, Z.; Zhang, L. Numerical Investigation on the Characteristics of Flow and Heat Transfer Enhancement by Micro Pin-Fin Array Heat Sink with Fin-Shaped Strips. *Chemical Engineering and Processing—Process Intensification* **2021**, *160*, 108273. DOI: 10.1016./j.cep.2020.108273.
5. Van Thin, D. V.; Sang, P. L. H.; Tho, L. V. Analysis of the Fluid Flow Characteristics in Subchannels of VVER-1000 Reactor's Fuel Assemblies by CFD Method. *Nukleon* **2016**, *189*. http://nuklearis.hu/sites/default/files/nukleon/9_1_189_Thin.pdf.
6. Lin, C.-H.; Yen, C.-H.; Ferng, Y.-M. CFD Investigating the Flow Characteristics in a Triangular-Pitch Rod Bundle Using Reynolds Stress Turbulence Model. *Annals of Nuclear Energy* **2014**, *65*, 357–364. DOI: 10.1016/j.anucene.2013.11.023.
7. Islam, M. S.; Khan, A. H. Thermal-Hydraulic Analysis of Fuel Rod of a TRIGA Mark II Research Reactor. *International Journal of Engineering and Technology* **2020**, *9* (1), 69–76. DOI: 10.14419/ijet.v9i1.30035.
8. Ahmed, F.; Abir, M. A.; Bhowmik, P. K.; Deshpande, V.; Mollah, A. S. Thermohydraulic Performance of Water Mixed Al_2O_3, TiO_2 and Graphene-Oxide Nanoparticles for Nuclear Fuel Triangular Subchannel. *Thermal Science and Engineering* **2021**, *24*, 100929. DOI: 10.1016/j.tsep.2021.100929.
9. Thakare, H. R.; Parekh, A. D. CFD Analysis of Energy Separation of Vortex Tube Employing Different Gases, Turbulence Models and Discretisation Schemes. *International Journal of Heat and Mass Transfer* **2014**, *78*, 360–70. DOI: 10.1016/j.ijheatmasstransfer.2014.06.083.
10. Anderson, J. D. Governing Equations of Fluid Dynamics. In *Computational Fluid Dynamics*, J.F. Wendt, Ed.; Verlag Berlin Heidelberg: Germany, 2009; 15–51. https://www.eng.auburn.edu/~tplacek/courses/fluidsreview-1.pdf.
11. Kurganov, V. A. Pressure Drop, Single-Phase. *Thermopedia* **2011**. DOI: 10.1615/AtoZ.p.pressure_drop_single-phase.
12. Rehm, B.; Drilling Consultant; Haghshenas, A.; Paknejad, A. S.; Schubert, J. CHAPTER TWO—Situational Problems in MPD. In *Managed Pressure Drilling*, B. Rehm, J. Schubert, A. Haghshenas, A. S. Paknejad, J. Hughes, Eds.; Texas

A&M University: College Station, Texas, 2008; 39–80. DOI: 10.1016/B978-1-933762-24-1.50008-5.
13. Thome, J. R. Two-Phase Pressure Drop. In *Engineering Data Book III*; Wolverine Tube Inc.: 2006, 13(1–34).
14. Shaheed, R.; Mohammadian, A.; Gildeh, H. K. A Comparison of Standard k–ε and Realizable k–ε Turbulence Models in Curved and Confluent Channels. *Environmental Fluid Mechanics* **2019**, *19*, 543–568. DOI: 10.1007/s10652-018-9637-1.
15. Baker, C.; Johnson, T.; Flynn, D. C.; Hemida, H.; Quinn, A.; Soper, D.; Sterling, M. Chapter 4—Computational Techniques. In *Train Aerodynamics*, Butterworth-Heinemann: 2019, 53–71. DOI: 10.1016/B978-0-12-813310-1.00004-6.
16. International Atomic Energy Agency. *Status Report 108—VVER-1200 (V-491) (VVER-1200 (V-491))*; International Atomic Energy Agency: Vienna, 2011. https://aris.iaea.org/PDF/VVER-1200(V-491).pdf.
17. Sabhasachi, S.; Koushik, R.; Souvik, R.; Asfakur, R. M.; Zahid, H. M. Rooppur Nuclear Power Plant: Current Status and Feasibility. *Strojnícky časopis—Journal of Mechanical Engineering* **2018**, *68* (3), 167–182. DOI: 10.2478/scjme-2018-0033.
18. *ansys*; ansys: 2023. https://www.ansys.com/.